6748 Vol. 45, No. 24 / 15 December 2020 / Optics Letters Letter

Optics Letters

Observation of second-order interference beyond the coherence time with true thermal photons

Gyu-Hyeok Lee,[1,2] Dong-Gil Im,[1] Yosep Kim,[1] U-Shin Kim,[1] and Yoon-Ho Kim[1,*]

[1]Department of Physics, Pohang University of Science and Technology (POSTECH), Pohang, 37673, Republic of Korea
[2]e-mail: gyuhyeoklee@gmail.com
*Corresponding author: yoonho72@gmail.com

Received 22 October 2020; revised 19 November 2020; accepted 20 November 2020; posted 22 November 2020 (Doc. ID 413287); published 14 December 2020

It has recently been shown that counter-intuitive Franson-like second-order interference can be observed with a pair of classically correlated pseudo thermal light beams and two separate unbalanced interferometers (UIs): the second-order interference visibility remains fixed at 1/3 even though the path length difference in each UI is increased significantly beyond the coherence length of the pseudo thermal light [Phys. Rev. Lett. 119, 223603 (2017)]. However, as the pseudo thermal beam itself originated from a long-coherence laser (and by using a rotating ground disk), there exists the possibility of a classical theoretical model to account for second-order interference beyond the coherence time on the long coherence time of the original laser beam. In this work, we experimentally explore this counter-intuitive phenomenon with a true thermal photon source generated via quantum thermalization, i.e., obtaining a mixed state from a pure two-photon entangled state. This experiment not only demonstrates the unique second-order coherence properties of thermal light clearly but may also open up remote sensing applications based on such effects.

https://doi.org/10.1364/OL.413287

Optical interferometry has been a key workhorse in various fields of astronomy, metrology, communication, information processing, and fundamental studies. Especially, the second-order intensity correlation between two light beams measured with two detectors, commonly known as Hanbury Brown and Twiss (HBT) interferometry [1], has prompted novel understanding of optical coherence [2–4] and marked the beginning of quantum optics [5]. Second-order interference based on HBT interferometry is in fact at the heart of numerous modern applications of quantum optics, namely, quantum interferometry for fundamental studies [6–9], characterization of single-photon sources [10,11], quantum imaging [12–15], photonic quantum gate operation [16–20], quantum optical metrology [21–26], quantum communication [27], etc.

It is commonly understood that the coherence time of light, classically determined by the spectral bandwidth from the Wiener–Khinchin theorem, is the timescale over which interference can be observed [28], although the N-photon coherence time in quantum interferometry ($N \geq 3$) depends on the number of interfering photons and the specific measurement scheme used to detect the photons [29]. Surprisingly and seemingly in contradiction to the common understanding of temporal coherence [28,30,31], the intensity correlation between the outputs of two unbalanced interferometers (UIs) with two classically correlated beams of pseudo thermal light at the input exhibits unique second-order interference that does not degrade with the UI path length difference increase [32–34]. In fact, the second-order interference visibility is shown to be fixed at 1/3 no matter how much the path length difference in each UI is increased beyond the coherence length of the pseudo thermal light [32–34]. However, for the experimental observation in Ref. [33], the pseudo thermal light source was implemented by making use of a long-coherence laser beam and a rotating ground disk. This method merely gives an arbitrary phase to the laser beam depending on the rotating speed of the ground disk, so a residual coherence laser beam could in principle be measured with extremely fast detectors. Thus, there exists the possibility of a classical theoretical model to account for second-order interference beyond the coherence time on the long coherence time of the original laser beam. In this work, we experimentally explore the counter-intuitive second-order interference, in which the interference visibility is completely irrespective of the path length differences, with a true thermal photon source generated via quantum thermalization, i.e., obtaining a mixed state from a pure two-photon entangled state [35,36]. The thermal (mixed) state of the photon was obtained by tracing out one subsystem of a pure two-photon entangled state generated via the atomic spontaneous four-wave mixing (SFWM) process. This experiment not only clarifies the unique second-order coherence properties of true thermal (mixed state) photons but may also open up remote metrology applications based on such properties, i.e., coherence-time-insensitive and turbulence-robust second-order interference of thermal photons [37–39].

The overall experimental schematic for observing second-order interference beyond the coherence time with true thermal light is shown in Fig. 1. The true thermal light beam, labeled as the idler in Fig. 1, is generated from spontaneous emission of ^{87}Rb atoms. The thermal idler beam is then split into two

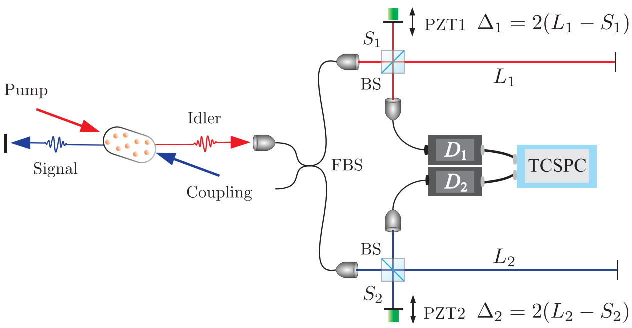

Fig. 1. Experimental schematic. The true thermal photon source is generated via quantum thermalization, i.e., obtaining a mixed state from a pure two-photon entangled state through atomic cascade decay. In unbalanced interferometers (UIs), the path length differences Δ_1 and Δ_2 are significantly larger than the coherence length of the thermal light. BS, beam splitter; FBS, fiber beam splitter; PZT, piezoelectric transducer; TCSPC, time-correlated single-photon counting module.

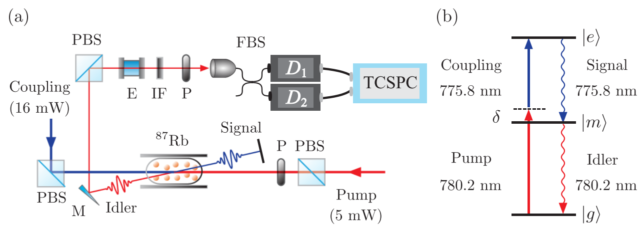

Fig. 2. (a) Schematic for a true thermal photon source generated via quantum thermalization, i.e., obtaining a mixed state from a pure two-photon entangled state through atomic cascade decay. The pump and coupling beams excite the ^{87}Rb atoms from the ground state $|g\rangle$ to the excited state $|e\rangle$ via the two-photon transition shown in (b). Due to the ladder-type spontaneous four-wave mixing process, the energy–time entangled two-photon pure state is generated. The signal photon is discarded so that the resulting quantum state of the idler photon is thermalized. E, fused-silica etalon filter; IF, interference filter; P, Glan–Thompson polarizer; M, mirror. (b) Energy level diagram ($\delta = 900$ MHz, $|g\rangle = |5S_{1/2}, F = 2\rangle$, $|m\rangle = |5P_{3/2}, F' = 3\rangle$, $|e\rangle = |5D_{5/2}, F'' = 4\rangle$).

correlated beams of light with a fiber beam splitter (FBS), and these beams are fed into two separate UIs. Here, the long and short paths are noted as $L_1(L_2)$ and $S_1(S_2)$ for the UIs, respectively. The path length differences $\Delta_1 = 2(L_1 - S_1)$ and $\Delta_2 = 2(L_2 - S_2)$ are significantly larger than the coherence length of the thermal idler beam so that there is no first-order interference observed at two detectors D_1 and D_2. Note that this condition is similar to that of the entangled-photon-based Franson interference [8,9]. When the coincidence between the two detectors is measured, however, unique second-order interference of thermal light emerges [33]. In the photon picture, the emergence of second-order interference in this setup can be explained as quantum interference of four two-photon probability amplitudes due to the transit of the photons through the path-pairs (L_1, L_2), (S_1, S_2), (L_1, S_2), and (S_1, L_2) [32,34]. The indistinguishability condition requires that the length differences $|L_1 - L_2|$ and $|S_1 - S_2|$ be kept less than the coherence length of the thermal light.

The coincidence between the two detectors D_1 and D_2 is proportional to the second-order correlation function $g^{(2)}(t_1, t_2)$, which is calculated to be

$$g^{(2)}(t_1, t_2) \propto 2 + \gamma\left(1 + \cos\left(\frac{\omega}{c}(\Delta_1 - \Delta_2)\right)\right), \quad (1)$$

where ω is the central frequency of thermal light, and c is the speed of light in vacuum. The parameter γ represents experimental degradation of the measured autocorrelation function of thermal light (i.e., $\gamma = g^{(2)}_{\rm auto}(0) - 1$) and is included to reflect the limited timing resolution of the detectors. Ideally, for the thermal light, $g^{(2)}_{\rm auto}(0) = 2$ so that the second-order interference visibility is fixed at 1/3 completely irrespective of the path length differences in the UIs.

For generating the true thermal statistics of photons, we make use of quantum thermalization: while the two-photon entangled state is a pure state, the respective states of the subsystems (i.e., the signal and idler photons) are not. The quantum states of the individual signal and idler photons are both in thermal (mixed) states [35,36]. The detailed experimental setup for true thermal photon generation via quantum thermalization, i.e., obtaining a mixed state from a pure two-photon entangled state through atomic cascade decay, is shown in Fig. 2(a). The horizontally polarized pump beam and vertically polarized coupling beam propagate in opposite directions through the Rb vapor cell, which is heated at 60°C and covered by a μ metal shield. The two beams generate energy–time entangled photon pairs, the signal and idler photons, via the ladder-type SFWM process; see Fig. 2(b) for the energy level diagram. The SFWM photon pair itself is in a two-mode squeezed state, but if one subsystem is traced out, the other subsystem is in a thermal (mixed) state [35,36]. According to Ref. [35], this process is "thermalization that is intrinsically quantum mechanical." In experiment, only the idler photon in a thermal (mixed) state is collected and used for the experiment. The angle between the idler photon and the pump laser beam is 1.43°. To further minimize the effect of the scattered photons from the pump laser, a solid etalon (E) of 1 GHz bandwidth and an interference filter (IF) of 1 nm bandwidth are used. Also, the horizontal polarization components are filtered out by using a polarizing beam splitter (PBS) and a Glan–Thompson polarizer (P).

The thermal nature of the idler photon is measured with the HBT setup in Fig. 2(a), and the result of the HBT autocorrelation measurement, $g^{(2)}_{\rm auto}(0)$, is shown in Fig. 3. The experimental data show that $g^{(2)}_{\rm auto}(0) = 1.74$, which is less than the ideal value of two. This is due to the relatively large bandwidth of the idler photon with respect to the timing resolution of the detectors (Excelitas, SPCM model) [40,41]. By deconvoluting the obtained autocorrelation function with the detectors' temporal response function, the autocorrelation function for the idler photon can be obtained [42,43]. The deconvoluted autocorrelation function for the idler photon shows $g^{(2)}_{\rm auto}(0) = 1.99$, confirming the thermal nature of the idler photon. The coherence time τ_c of the thermal idler photon is estimated to be $\tau_c = 1.63$ ns, and the corresponding coherence length is $c\tau_c = 0.48$ m. Note that the coherence time of pseudo thermal light is dependent on the rotation speed of the ground disk, so the typical coherence time of pseudo thermal light is between a few microseconds to milliseconds [15,33]. Since the atomic thermal light source based on quantum thermalization offers almost ideal thermal light, $g^{(2)}_{\rm auto}(0) = 1.99$, with a very large bandwidth (i.e., very short coherence time), it is well-suited for thermal-light-based remote sensing applications [37–39].

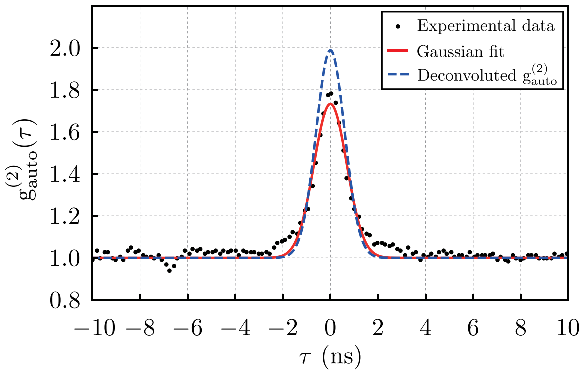

Fig. 3. Autocorrelation $g^{(2)}_{auto}(\tau)$ of the idler photon. The experimental data show $g^{(2)}_{auto}(0) = 1.74$. The blue dashed line shows the autocorrelation function after deconvoluting the detectors' timing resolution, $g^{(2)}_{auto}(0) = 1.99$, confirming the thermal nature of the idler photon. The coherence time τ_c of the thermal idler photon is estimated to be $\tau_c = 1.63$ ns, and the corresponding coherence length is $c\tau_c = 0.48$ m.

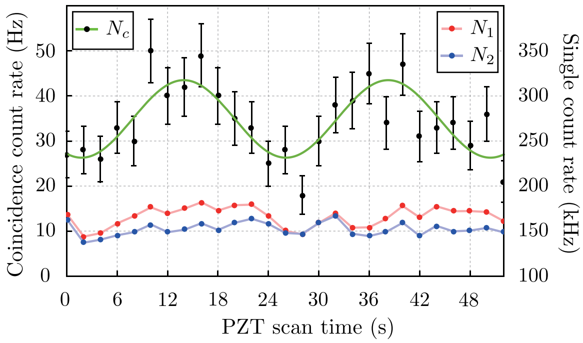

Fig. 4. Path length difference of $\Delta_1 = \Delta_2 = 1$ m is larger than $c\tau_c = 0.48$ m of the thermal idler photon. No first-order interference occurs when Δ_1 is decreased at the speed of 11.9 nm/s, but second-order interference occurs at the visibility of $25.2 \pm 2.5\%$.

We now show the results of the second-order interference experiment of the setup shown in Fig. 1 with the true thermal (mixed) photon source shown in Figs. 2 and 3. The second-order correlation function is experimentally obtained by measuring the coincidence count rate N_c with a narrow coincidence window of 1 ns at the equal detection time. The single count rates, N_1 and N_2, of the detectors D_1 and D_2 as well as the coincidence count rate, N_c, are measured while scanning PZT1, thereby scanning the path length difference Δ_1, in Fig. 1. PZT1 is scanned by applying a linearly increasing voltage at the rate of 0.10 V/s, corresponding to the scan speed of 11.9 nm/s. Considering the coherence length of the thermal light, $c\tau_c = 0.48$ m, the path length differences are set at $\Delta_1 = \Delta_2 = 1$ m so that there is no first-order interference. As seen in Fig. 4, the single count rates show no interference features. Small fluctuations on the single count rates come from the power fluctuation of the frequency-locked pump and coupling lasers. The coincidence count exhibits sinusoidal interference fringes at the visibility of $25.2 \pm 2.5\%$. Although the theoretical maximum visibility according to Eq. (1) is 33.3%, due to the fact that the measured $g^{(2)}_{auto}(0) = 1.74$ in Fig. 3, the maximum

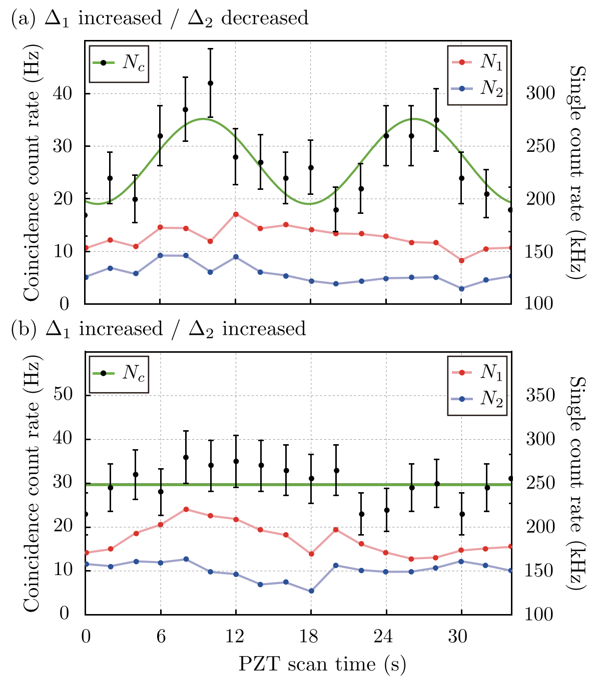

Fig. 5. Path length differences are set at $\Delta_1 = \Delta_2 = 1$ m, and both Δ_1 and Δ_2 are scanned at the speed of 11.9 nm/s. (a) When Δ_1 and Δ_2 are scanned in opposite directions, second-order interference is observed at the visibility of $29.5 \pm 4.1\%$. (b) When Δ_1 and Δ_2 are scanned in the same direction, no second-order interference is observed, as expected from Eq. (1).

observable second-order interference visibility reduces to 27%. Thus, our experimental observation is consistent with Eq. (1).

Another interesting feature of this experiment is that, even though the experimental setup in Fig. 1 resembles the entangled-photon-based Franson interferometer [8,9], the phase response of the interference is quite different. For the Franson interferometer, the second-order interference is dependent on the phase sum $\Delta_1 + \Delta_2$, but for the thermal photon, the second-order interference is dependent on the phase difference $\Delta_1 - \Delta_2$, as shown in Eq. (1). To explore this feature, we scan PZT1 and PZT2 in the same and in the opposite directions at the same speed of 11.9 nm/s. As shown in Fig. 5(a), when the path length differences are oppositely scanned, second-order interference with the visibility of $29.5 \pm 4.1\%$ is observed. Since the thermal photon second-order interference is related to the phase difference, $\Delta_1 - \Delta_2$, scanning Δ_1 and Δ_2 in the opposite directions at the same speed is effectively the same as scanning only Δ_1 at twice the speed, as evidenced in the horizontal axis of Fig. 5(a). When both Δ_1 and Δ_2 are scanned in the same direction, second-order interference does not appear since the phase difference $\Delta_1 - \Delta_2$ is constant, as confirmed in the experimental data shown in Fig. 5(b).

Perhaps the most unique feature of thermal photon second-order interference in the setup in Fig. 1 is that the interference visibility is completely irrespective of the path length differences in the UIs. To probe this feature for the true thermal photon used in our experiment, we measured thermal photon second-order interference for increased path length differences, $\Delta_1 = \Delta_2 = 1.5$ m and $\Delta_1 = \Delta_2 = 2$ m, by scanning Δ_1 at the speed of 13.2 nm/s. As shown in the experimental data in Fig. 6,

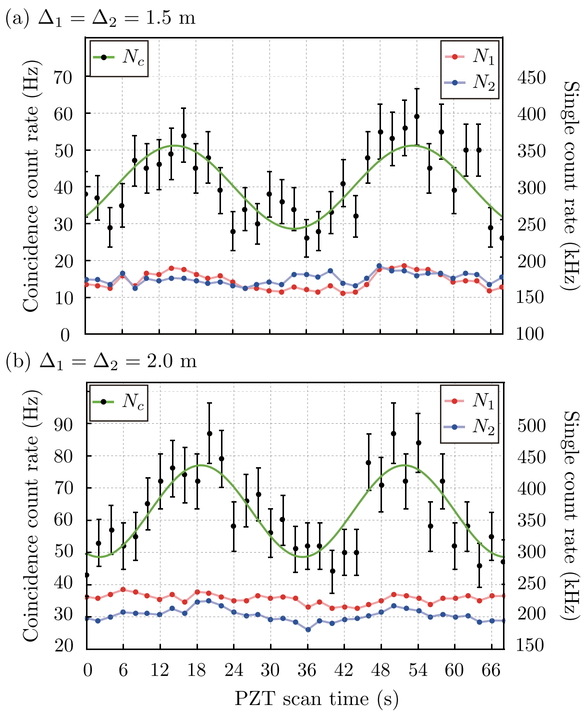

Fig. 6. Path length differences $\Delta_1 = \Delta_2$ are set to be (a) 1.5 m and (b) 2.0 m. Δ_1 is decreased at the speed of 13.2 nm/s. The second-order interference visibility is (a) $27.7 \pm 4.4\%$ and (b) $24.2 \pm 4.4\%$.

thermal photon second-order interference is still observed irrespective of the path length differences.

In summary, we have experimentally demonstrated counter-intuitive second-order interference beyond the coherence time, in which the interferometric path length difference is much larger than the coherence length of the light, with a true thermal photon source generated via quantum thermalization, i.e., obtaining a mixed state from a pure two-photon entangled state. The thermal (mixed) state of the photon was obtained by tracing out one subsystem of a pure two-photon entangled state generated via the atomic SFWM process. In addition to the fundamental importance to broader understanding of optical coherence, the second-order interference effect beyond the coherence time reported in this work could have significant remote sensing applications, as the thermal light second-order interference has some inherent robustness to atmospheric turbulence [38,44,45].

Funding. National Research Foundation of Korea (2019R1A2C3004812); Information Technology Research Center (IITP-2020-0-01606); Agency for Defense Development (UG190028RD).

Disclosures. The authors declare no conflicts of interest.

REFERENCES

1. R. Hanbury Brown and R. Q. Twiss, Nature **177**, 27 (1956).
2. E. M. Purcell, Nature **178**, 1449 (1956).
3. B. L. Morgan and L. Mandel, Phys. Rev. Lett. **16**, 1012 (1966).
4. H. J. Kimble, M. Dagenais, and L. Mandel, Phys. Rev. Lett. **39**, 691 (1977).
5. R. J. Glauber, Phys. Rev. Lett. **10**, 84 (1963).
6. C. K. Hong, Z. Y. Ou, and L. Mandel, Phys. Rev. Lett. **59**, 2044 (1987).
7. Y. H. Shih and C. O. Alley, Phys. Rev. Lett. **61**, 2921 (1988).
8. J. D. Franson, Phys. Rev. Lett. **62**, 2205 (1989).
9. O. Kwon, K.-K. Park, Y.-S. Ra, Y.-S. Kim, and Y.-H. Kim, Opt. Express **21**, 25492 (2013).
10. C. K. Hong and L. Mandel, Phys. Rev. Lett. **56**, 58 (1986).
11. G. Noh, D. Choi, J.-H. Kim, D.-G. Im, Y.-H. Kim, H. Seo, and J. Lee, Nano Lett. **18**, 4710 (2018).
12. T. B. Pittman, Y. H. Shih, D. V. Strekalov, and A. V. Sergienko, Phys. Rev. A **52**, R3429 (1995).
13. M. D'Angelo, Y.-H. Kim, S. P. Kulik, and Y. Shih, Phys. Rev. Lett. **92**, 233601 (2004).
14. F. Ferri, D. Magatti, A. Gatti, M. Bache, E. Brambilla, and L. A. Lugiato, Phys. Rev. Lett. **94**, 183602 (2005).
15. Y.-W. Cho, J.-E. Oh, and Y.-H. Kim, Opt. Express **20**, 5809 (2012).
16. E. Knill, R. Laflamme, and G. J. Milburn, Nature **409**, 46 (2001).
17. M. Koashi, T. Yamamoto, and N. Imoto, Phys. Rev. A **63**, 030301 (2001).
18. T. B. Pittman, B. C. Jacobs, and J. D. Franson, Phys. Rev. Lett. **88**, 257902 (2002).
19. Y. Kim, Y.-S. Kim, S.-Y. Lee, S.-W. Han, S. Moon, Y.-H. Kim, and Y.-W. Cho, Nat. Commun. **9**, 192 (2018).
20. Y.-W. Cho, Y. Kim, Y.-H. Choi, Y.-S. Kim, S.-W. Han, S.-Y. Lee, S. Moon, and Y.-H. Kim, Nat. Phys. **15**, 665 (2019).
21. M. B. Nasr, B. E. A. Saleh, A. V. Sergienko, and M. C. Teich, Phys. Rev. Lett. **91**, 083601 (2003).
22. Y.-S. Kim, O. Kwon, S. M. Lee, J.-C. Lee, H. Kim, S.-K. Choi, H. S. Park, and Y.-H. Kim, Opt. Express **19**, 24957 (2011).
23. S. Oppel, T. Büttner, P. Kok, and J. von Zanthier, Phys. Rev. Lett. **109**, 233603 (2012).
24. A. Jechow, M. Seefeldt, H. Kurzke, A. Heuer, and R. Menzel, Nat. Photonics **7**, 973 (2013).
25. D. A. Kalashnikov, A. V. Paterova, S. P. Kulik, and L. A. Krivitsky, Nat. Photonics **10**, 98 (2016).
26. K. Y. Spasibko, D. A. Kopylov, V. L. Krutyanskiy, T. V. Murzina, G. Leuchs, and M. V. Chekhova, Phys. Rev. Lett. **119**, 223603 (2017).
27. S. Wengerowsky, S. K. Joshi, F. Steinlechner, H. Hübel, and R. Ursin, Nature **564**, 225 (2018).
28. S. P. Davis, M. C. Abrams, and J. W. Brault, *Fourier Transform Spectrometry* (Academic, 2001).
29. Y.-S. Ra, M. C. Tichy, H.-T. Lim, O. Kwon, F. Mintert, A. Buchleitner, and Y.-H. Kim, Nat. Commun. **4**, 2451 (2013).
30. S.-Y. Baek, O. Kwon, and Y.-H. Kim, Jpn. J. Appl. Phys. **46**, 7720 (2007).
31. O. Kwon, Y.-S. Ra, and Y.-H. Kim, Opt. Express **17**, 13059 (2009).
32. V. Tamma and J. Seiler, New J. Phys. **18**, 032002 (2016).
33. Y.-S. Ihn, Y. Kim, V. Tamma, and Y.-H. Kim, Phys. Rev. Lett. **119**, 263603 (2017).
34. V. Tamma, Phys. Scr. **93**, 124010 (2018).
35. B. Yurke and M. Potasek, Phys. Rev. A **36**, 3464 (1987).
36. D. V. Strekalov, Y.-H. Kim, and Y. Shih, Phys. Rev. A **60**, 2685 (1999).
37. M. D'Angelo, A. Mazzilli, F. V. Pepe, A. Garuccio, and V. Tamma, Sci. Rep. **7**, 2247 (2017).
38. F. V. Pepe, G. Chilleri, G. Scala, D. Triggiani, Y.-H. Kim, and V. Tamma, "Quantum-inspired distance sensing using thermal light second-order interference," arXiv:2011.05224 (2020).
39. C.-H. Lee, Y. Kim, V. Tamma, and Y.-H. Kim are preparing a manuscript to be titled "Demonstration of distance sensing using thermal light second-order interference."
40. B. Blauensteiner, I. Herbauts, S. Bettelli, A. Poppe, and H. Hübel, Phys. Rev. A **79**, 063846 (2009).
41. Y.-S. Ihn, K.-K. Park, Y. Kim, Y.-T. Chough, and Y.-H. Kim, J. Opt. Soc. Am. B **34**, 2352 (2017).
42. A. Dussaux, T. Passerat de Silans, W. Guerin, O. Alibart, S. Tanzilli, F. Vakili, and R. Kaiser, Phys. Rev. A **93**, 043826 (2016).
43. J. Mika, L. Podhora, L. Lachman, P. Obšil, J. Hloušek, M. Ježek, R. Filip, and L. Slodička, New J. Phys. **20**, 093002 (2018).
44. R. E. Meyers and K. S. Deacon, Entropy **17**, 1508 (2015).
45. Y. Shih, Technologies **4**, 39 (2016).